

Ultra-low noise quantum memory for quasi-deterministic single photons generated by Rydberg collective atomic excitations

L. Heller,^{1,*} J. Lowinski,^{1,*} K. Theophilo,¹ A. Padrón-Brito,¹ and H. de Riedmatten^{1,2}

¹*ICFO-Institut de Ciències Fotoniques, The Barcelona Institute of Science and Technology*

²*ICREA-Institució Catalana de Recerca i Estudis Avançats, 08015 Barcelona, Spain*

We demonstrate the storage and retrieval of an on-demand single photon generated by a collective Rydberg excitation in an ultra-low noise Raman quantum memory located in a different cold atomic ensemble. We generate single photons on demand by exciting a cold cloud of Rubidium atoms off resonantly to a Rydberg state, with a generation probability up to 15 % per trial. We then show that the single photons can be stored and retrieved with an efficiency of 21 % and a noise floor of $p_n = 2.3(3) \times 10^{-4}$ per trial in the Raman quantum memory. This leads to a signal-to-noise ratio ranging from 11 to 26 for the retrieved single photon depending on the input photon generation probability, which allows us to observe significant antibunching. We also evaluate the performances of the Raman memory as built-in unbalanced temporal beam splitter, tunable by varying the write-in control pulse intensity. In addition, we demonstrate that the Raman memory can be used to control the single-photon waveshape. These results are a step forward in the implementation of efficient quantum-repeater links using single-photon sources.

I. INTRODUCTION

The development of quantum networks [1] is one of the most active branches of quantum technologies. A fundamental step towards long distance quantum communications would be the realization of efficient quantum repeaters [2–4] that would allow the distribution of entanglement over distances longer than what is achievable with direct photon transmission. Near term quantum repeaters are based on heralded entanglement between remote quantum memories that form an elementary repeater link and on entanglement swapping between the elementary links to extend the entanglement distance. Various platforms have been considered as quantum memories for quantum repeaters, including single atoms [5, 6] or ions [7–10], cold atomic clouds [11–17] and solid-state systems such as color centers in diamond [18, 19] or rare-earth doped solids [20–25]. Ensemble-based approaches are promising for reaching high-rate quantum repeaters because they enable large multiplexing, which increases the rate of entanglement in elementary links proportionally to the number of stored modes [16, 24, 26–30].

To date, most of the early demonstrations of quantum repeater links with ensemble-based quantum memories are based on probabilistic light-matter entanglement sources, e.g. based on emissive quantum memories using spontaneous Raman scattering in atomic clouds [12–14, 17, 31], following the DLCZ proposal, or by using read-write quantum memories combined with spontaneous parametric down-conversion sources [24, 25]. However, this type of probabilistic sources leads to limitations due to a trade-off between excitation probability and fidelity of the generated state. To keep the errors due to the generation of multiple pairs low, and therefore the fi-

delity high, the generation probability must remain low. This trade-off leads to low success probability per trial (especially for multiple-link repeaters), which limits the overall high-fidelity entanglement rate [4].

A quantum repeater architecture based on the use of deterministic single photons and absorptive ensemble-based quantum memories was proposed to overcome this limitation [32]. In this scheme, each node consists of a deterministic single-photon source and a quantum memory. The single photon is sent on a beam splitter (BS) and one output of the BS is directed towards the quantum memory while the other output is converted to telecom wavelength and sent to a central station where it is mixed with the photonic mode from another distant quantum node. It has been shown that heralded single photons (generated from probabilistic sources) can be stored in quantum memories [33] with up to 87 % storage and retrieval efficiency [15, 34]. Hence, the main challenge of this scheme compared to schemes using probabilistic sources is to generate memory-compatible indistinguishable single photons on demand with high efficiency. In addition, the quantum memory should feature very low noise in order not to degrade the single photon properties.

Several approaches have been demonstrated to generate on-demand single photons using single emitters such as quantum dots, single molecules and color centers in diamond. However, most of these photons are not resonant with quantum memories and have a bandwidth much larger than the one of long-lived quantum memories. While progress has been made recently to interface photons from quantum dots and molecules to atomic vapors or rare-earth doped solids [35–38], so far high efficiency and long-lived storage of these photons has not been demonstrated. Single trapped atoms can be used to generate directly resonant and memory-compatible photons that have been interfaced with a BEC quantum memory [39], however, the efficient photon generation in a single mode requires placing the atom in a high-finesse

* These two authors contributed equally

cavity, which represents an experimentally complex task. In recent years, several experiments have shown that ensembles of Rydberg atoms could serve as a source of on-demand narrow-band [40–43] indistinguishable single photons [44–46]. This approach has the advantage that no high-finesse cavity is required, due to the collective nature of the single photon generation.

In this paper, we demonstrate the storage and retrieval of an on-demand single photon generated by a collective Rydberg excitation on a ultra-low noise Raman quantum memory located in a different cold atomic ensemble. We show that the single photons can be stored and retrieved with a signal-to-noise ratio (SNR) up to 26, preserving strong antibunching. We also evaluate the performance of the built-in temporal beam splitter offered by the Raman memory. In addition, we demonstrate that the Raman memory can be used to control the single photon waveshape. These results show that single photons generated on demand by Rydberg atoms can be stored in an atomic quantum memory, which is an important step towards the implementation of efficient quantum-repeater links using single-photon sources.

II. EXPERIMENTAL SETUP

Our experimental setup comprises of two ensembles of cold ^{87}Rb atoms situated in the same laboratory connected via 12 m of optical fiber cable. One of them is used to generate single photons in a quasi-deterministic way by exploiting the strong dipole-dipole interaction between Rydberg states (the source). Another is used to store and on-demand retrieve the generated photons in an atomic Raman memory.

In the first step of the generation protocol we excite the ensemble from its ground state $|g_s\rangle = |5S_{1/2}, F = 2\rangle$ to a Rydberg state $|r\rangle = |90S_{1/2}\rangle$, see Fig. 1(d), via a two-photon excitation. We send a weak coherent probe pulse Ω_p and a strong counter-propagating coupling pulse $\Omega_c \approx 6\text{ MHz}$, see Fig. 1(a). The probe light at a wavelength of 780 nm is red-detuned by -40 MHz from the transition to the excited state $|e_s\rangle = |5P_{3/2}, F = 3\rangle$. The coupling light is tuned such that the two-photon transition is resonant with the transition $|g_s\rangle \rightarrow |r\rangle$.

The number of generated Rydberg excitations is strongly limited due to the dipole blockade [47]. The blockade is a result of the strong dipole-dipole interaction between Rydberg states, which prevents a simultaneous excitation of two Rydberg atoms, if they are closer than a distance called the blockade radius. Then, if the interaction region is smaller than the volume given by the blockade radius, only one atomic excitation will be created in state $|r\rangle$ - this is called the fully blockaded regime. The Rydberg excitation is shared between all the atoms in the blockade region, forming a collective quantum superposition, termed Rydberg spin wave.

With a delay of 1 μs , a second coupling pulse is sent resonantly to the $|r\rangle \rightarrow |e_s\rangle$ transition, mapping the Rydberg spin wave onto the excited state $|e_s\rangle$ and triggering the collective emission of a single photon at 780 nm.

The photon is emitted in the input mode and in forward direction thanks to collective atomic interference. It is then separated from the coupling light by a dichroic mirror and a band-pass filter, before being collected into a polarization-maintaining single-mode fiber. An electronic trigger is sent to the memory to signal each photon generation attempt.

The generated photon is guided to the second atomic ensemble, the memory. The frequency of the photon is, however, not compatible with the transitions used in the memory, so it is shifted by -320 MHz with an acousto-optic modulator (AOM). As a result, the photon is now red-detuned with respect to the $|g_m\rangle \rightarrow |e_m\rangle$ transition.

The Raman memory relies on coherent, adiabatic absorption of the incoming single photon [48]. A storage attempt starts with sending a control write-in pulse Ω_W coupling states $|s\rangle = |5S_{1/2}, F = 1, m_F = 0\rangle$ and $|e_m\rangle = |5P_{3/2}, F = 2, m_F = +1\rangle$ off-resonantly by $\delta = -52\text{ MHz}$, see Fig. 1(e). Since the write-in pulse is in two-photon resonance with the input photon, the incoming photon field is transferred to a collective atomic spin excitation on $|s\rangle$. Careful tuning of the control write-in pulse shape, power and timing with respect to the input photon is required to optimize the writing efficiency into the memory.

To retrieve the stored excitation, after a programmable delay, we send a read-out pulse Ω_R . The read-out pulse is in the same spatial mode as the write-in pulse with the same frequency detuning δ . Owing to the collective atomic interference, the photon is emitted in the input mode in forward direction and collected into a single-mode fiber. The bandwidth and the shape of the output photon are governed by the temporal profile and the power of the read-out pulse and can be tuned arbitrarily (see section III B).

The collected photons are guided to the detection setup. Depending on the measurement it is either a superconducting nanowire single-photon detector (SNSPD) or a Hanbury Brown-Twiss (HBT) setup comprised of a fiber-based beam splitter and two SNSPDs, see Fig. 1(c). We use HBT setup to measure photons autocorrelation.

For the source to produce single photons it is necessary to be in the fully blockaded regime or close to it. Moreover, the coherence time of the Rydberg transition should be much longer than the excitation pulse duration to keep the photon generation probability high. In our case, this means that the ensemble needs to be cold to limit the motional dephasing. Both are achieved in the preparation stage when we first load the atoms into a magneto-optical trap (MOT), later compress them and subsequently apply 7 ms of polarisation-gradient cooling. Finally the ensemble is prepared by optical pumping to its initial ground state $|g_s\rangle = |5S_{1/2}, F = 2\rangle$. A one-dimensional dipole trap is kept on during the whole process (with a beam waist of 34 μm at an angle of 22° with respect to the probe beam and a depth of 0.3 mK). The whole process results in a cloud with OD of 6 and a tem-

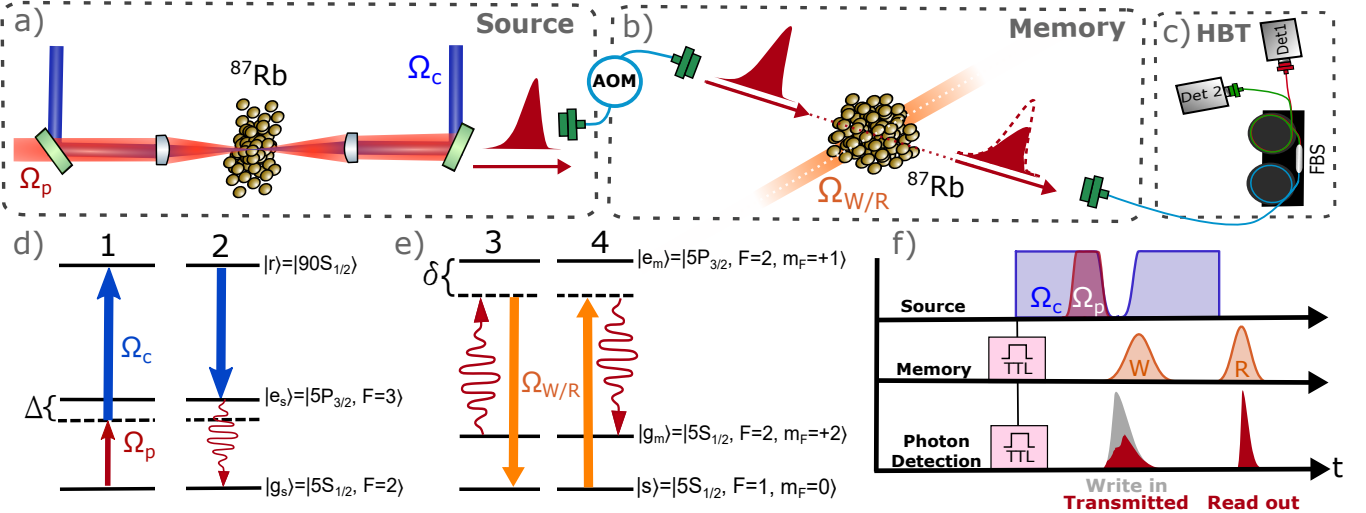


FIG. 1. A scheme of the experimental setup, the relevant atomic levels and the experimental sequence. (a) The source. The probe (Ω_p) and the counter-propagating coupling beam (Ω_c) are tightly focused in a cold cloud of Rubidium atoms to generate the input photon. (b) The memory. A write-in control beam pulse (Ω_W) maps the incoming photon to an atomic excitation in another cold cloud of Rubidium atoms. The excitation is retrieved with a read-out control beam pulse (Ω_R). (c) The retrieved photon is split in a fiber-based beam-splitter (FBS) and detected with two superconducting nanowire single-photon detectors SNSPD 1 and 2 performing, effectively, an HBT measurement. The relevant atomic levels for the photon generation (d) and for the photon storage (e) are also shown. A two-photon excitation (Ω_p and Ω_c , with $\Delta = -40$ MHz) creates a Rydberg spin wave in $|r\rangle$ (1) which is later mapped to the first excited state $|e_s\rangle$ and decays emitting a photon (2). The emitted photon is mapped with Ω_W to a ground-state spin wave in $|s\rangle$ (3) and later retrieved with Ω_R (4). (f) The pulse sequence. The whole experiment is synchronized with TTLs sent by the source at the beginning of each generation trial.

perature of $40\ \mu\text{K}$. Thanks to the dipole trap, the effective interaction region, given by the overlap between the probe beam and the atomic ensemble, is still larger but comparable to the $\sim 13\ \mu\text{m}$ of the blockade radius. The ensemble can be interrogated for $200\ \text{ms}$, limited by the population lifetime of the dipole trap ($400\ \text{ms}$), before another MOT reloading cycle has to be performed. During its interrogation time, the source attempts to generate a single photon every $4\ \mu\text{s}$ with generation probability $p_{\text{gen}} = 5\%$ to 15% . The photon generation and the characterization of their indistinguishability is described in more detail in [46].

For the memory, the OD of the ensemble and the cloud temperature are the main parameters governing the storage and retrieval efficiency and the storage time. To achieve a dense and cold ensemble the atoms are first loaded into a MOT for $10\ \text{ms}$ followed by $1.5\ \text{ms}$ of polarisation-gradient cooling. Later the memory is optically pumped to its initial ground state $|g_m\rangle = |5S_{1/2}, F = 2, m_F = +2\rangle$, in the presence of a homogeneous magnetic bias field oriented along the photon mode. Optical pumping is helpful to avoid beating between spin waves at different Zeeman sublevels. The whole process provides us a cloud with OD of 5 and a temperature of $30\ \mu\text{K}$. OD starts dropping after $1.2\ \text{ms}$ of interrogation time and the trapping cycle has to be repeated.

One of the main challenges of this study were long integration times which required good stability of both setups. This results mainly from two technical limitations. The first one are very different trapping cycles of the source and the memory making the overall duty cycle very low. The resulting repetition rate of the whole experiment is $5\ \text{kHz}$. The second one is the passive loss in the photon transmission which affects quadratically the coincidence probability in the HBT experiment. The total transmission from the output of the source to the detection setup, in the absence of atoms in the memory, is $10(1)\%$, limited by the fiber coupling after the source (0.4), the frequency-shifter AOM setup (0.62), the fiber coupling after the memory (0.83), the frequency-filtering cavity setup (0.65) and miscellaneous optical and polarisation-dependent losses (0.75). The transmission from the output of the source to the input of the quantum memory is 22 %. The SNSPDs have quantum efficiency $\sim 85\%$ and $3\ \text{Hz}$ of dark counts.

The limiting factor for the quality of the single photon retrieved from the quantum memory is the introduced technical noise, which affects its SNR. The main source of noise is the leakage of the memory control pulses which couple to the photon mode. An angle of 3 degrees between the photon mode and the coupling beam minimizes the spatial overlap and noise introduced by directional, forward scattering. The noise is further removed with a

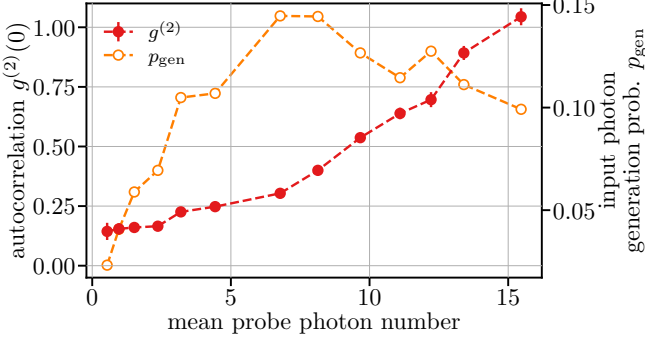


FIG. 2. Dependence of $g^{(2)}(0)$ and p_{gen} on mean probe photon number. p_{gen} follows the Rabi cycle decreasing for the largest values of the probe power while $g^{(2)}(0)$ grows monotonically up to 1.

home-built narrow-band Fabry-Perot filter cavity of 43.4 dB suppression (at the control pulse frequency). The remaining noise is composed of light leaking through the filter, inelastically scattered control light at the photon frequency and the detectors' dark counts.

III. RESULTS

In this section we study the single photon properties of the source photons which, further on, are used as the memory input photon. Secondly we discuss performance of the memory commenting on its tunability.

A. Photon Generation

The HBT setup is used to characterize the photons generated by the source. Photon arrival times at each SNSPD are recorded together with trigger times for each experimental trial. We compute the second order autocorrelation function as:

$$g^{(2)}(n) = \frac{c_{1,2}(n)}{p_1 p_2}, \quad (1)$$

where p_1 (p_2) is the probability of detection per trial with SNSPD 1 (2) and $c_{1,2}(n)$ is the probability of a coincidence between detections separated by n trials ($n = 0$ means that detections are taken within the same trial). All the probabilities are calculated within a detection time window at fixed delay after each trial trigger. We choose a 300 ns detection window which includes more than 95 % of the photon. For perfect single photons $g^{(2)}(0) = 0$. In practice, background noise or multiphoton components increase the $g^{(2)}(0)$. Emitted light remains non classical for $g^{(2)}(0) < 1$ and $g^{(2)}(0) = 0.5$ marks the limit between single and multi-photon states.

In our source we can change the emitted photon $g^{(2)}(0)$ within a range of 0.16 to 1 by varying the mean probe photon number, see Fig. 2. For smaller probe photon

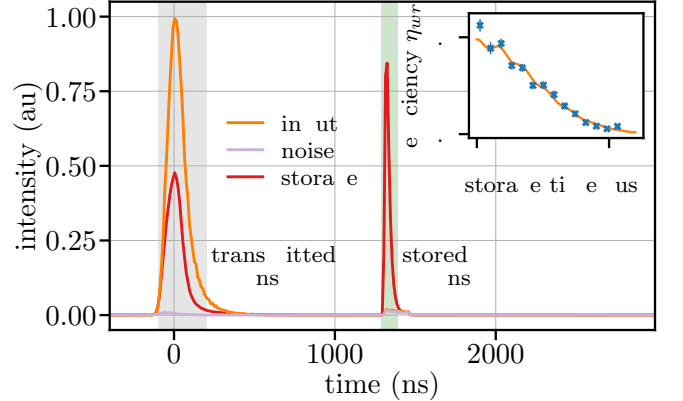


FIG. 3. Photon histogram observed at the SNSPDs after the memory. The orange histogram is the input photon alone with no storage attempt. The red histogram presents a storage attempt. The lavender histogram shows the noise without input photon, but with the atoms in the memory. The grey shaded area is the detection window for the input and transmitted photon and green shaded area is the detection window for the stored photon. The inset shows the storage efficiency as a function of storage time with the corresponding Gaussian fit e^{-t^2/τ^2} , where τ is the memory lifetime. The fit also includes an oscillatory term accounting for spin wave interference coming from residual population in $|5S_{1/2}, F = 2, m_F = 1\rangle$ (as an effect of imperfect Zeeman optical pumping) [49].

number values the increase of $g^{(2)}(0)$ is accompanied by an increase of the photon generation probability p_{gen} , which is defined as $p_{\text{gen}} = (p_1 + p_2)/\alpha$ where $\alpha = 0.21$ is the combined transmission and detection efficiency (of the source only - in this characterisation we detected photons right after the source). However, for larger probe photon number p_{gen} decreases in accordance with the Rabi cycle. Yet, this is not accompanied by the $g^{(2)}(0)$ which continues to grow up to 1, indicating the presence of multiphoton components. The reason for this behaviour is still under investigation and goes beyond the scope of this paper.

If not stated otherwise, for the following measurements we fix $g^{(2)}(0) \approx 0.23$ and $p_{\text{gen}} \approx 12\%$. The emitted photon has a steep leading edge followed by a slower exponential decay, with a FWHM of the entire photon of ~ 120 ns, see Fig. 3 at time zero.

B. Photon Storage

In this section we demonstrate that the memory can efficiently store the generated single photon. It also offers tunability in the storage and retrieval process.

To characterize the memory performance, we first measure the temporal histogram of photon counts in 3 different situations, as shown in Fig. 3. We first detect the input single photon (orange histogram) when no storage attempt is performed, i.e. with no atoms in the memory

but with control pulses. Then, a storage attempt is performed (red histogram) and one can see two peaks - the transmitted photon, which is the part of the input photon that is not absorbed in the storage attempt (counts in the 300 ns grey shaded window), and the stored photon, which is the excitation retrieved from a successful storage attempt (counts in the 100 ns green shaded window). Finally, we measure the noise (lavender histogram) by blocking the input photon while keeping all the control pulses on and the atomic cloud present. This last measurement should contain all the information about the noise present in the experiment, in particular the noise introduced by the control pulses. We measure a noise probability per trial within the storage window of $p_n = 2.3(3) \times 10^{-4}$, which, to our knowledge, is among the lowest reported in ground state spin-wave memories.

The input and the noise histograms serve as a reference to calculate the storage efficiency $\eta_{wr} = p_s/p_{in}$, where p_s and p_{in} are background-subtracted probabilities of detecting a stored photon (within the 100 ns detection window) and an input photon (within the 300 ns detection window), respectively. We also calculate the write-in efficiency defined as $\eta_w = (p_{in} - p_t)/p_{in}$, where p_t is the background-subtracted detection probability of a transmitted photon (within the 300 ns detection window). From these two quantities we infer the read-out efficiency $\eta_r = \eta_{wr}/\eta_w$. We obtain a maximum storage efficiency $\eta_{wr} \approx 21\%$ at a storage time of 1.2 μ s. For longer storage times the motional decoherence and the decoherence due to the stray magnetic field gradients limits the efficiency with a characteristic $1/e$ decay time of 30 μ s (see inset in Fig. 3).

For the measurement shown in Fig. 3, the SNR of the retrieved photon is 24(4). For different input number of photons, we measure SNR of up to 26 (see supplemental materials [50]). An interesting figure of merit is the μ_1 parameter, defined as $\mu_1 = p_n/\eta_{wr}$, which expresses the input number of photons required to have $\text{SNR} = 1$ at the output. In our case, we find $\mu_1 = 1.00(7) \times 10^{-3}$ (see supplemental materials [50]), which is more than two orders of magnitude lower than similar ground state quantum memories based on warm atomic vapors [51–53], and more than one order of magnitude lower than solid-state QMs based on rare-earth doped solids [33, 54].

A crucial requirement for a quantum memory is that it preserves the statistical properties of the stored photons. To show that our memory fulfills this criterion, we first adjust the mean probe photon number of the source to low values, resulting in a measured photon generation probability of $p_{gen} \approx 3.0(3)\%$ (see Fig. 2). With this setting, we expect the emitted photons to be strongly non-classical. To reduce the effect of experimental fluctuations, we collect data for 63 hours. We measure $g^{(2)}(0)$ of the input ($g^{(2)}(0) = 0.20(2)$), transmitted ($g^{(2)}(0) = 0.22(3)$) and stored photons ($g^{(2)}(0) = 0.34(7)$) and obtain values well below 0.5, see Fig. 4. It shows that the memory preserves the single photon nature of the input photon. One can see, however, that $g^{(2)}(0)$ of the stored

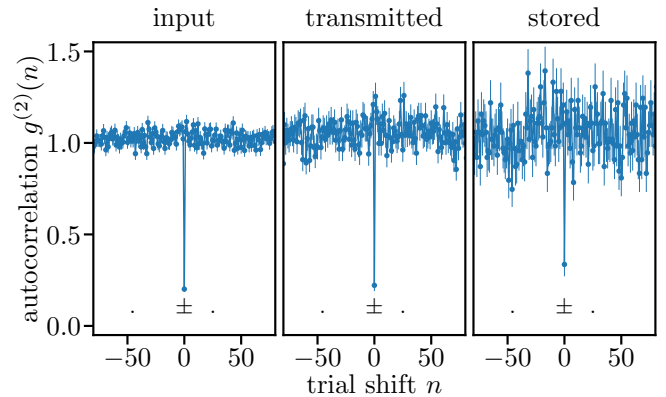


FIG. 4. Autocorrelation $g^{(2)}$ as a function of shift between trials n for the input, transmitted and stored photons. For trials separated by a shift $n \geq 1$ the clicks are uncorrelated yielding $g^{(2)}(n) = 1$. Coincidences clicks in the same trial, $n = 0$, are much less frequent asserting the photons anti-bunching.

photon is significantly larger than the $g^{(2)}(0)$ of the input photon. We expect that the main source of degradation of $g^{(2)}(0)$ is the uncorrelated noise introduced by the memory control pulses. We developed a simple model, discussed in the supplemental materials [50], to quantify the effect of uncorrelated noise on $g^{(2)}(0)$. The model predicts a $g_m^{(2)}(0) = 0.33(4)$ for stored photon taking into account a measured SNR of 11(2) and the measured input $g^{(2)}(0)$. For this data set, the model is in agreement with the measured data, within the error bars. We also performed several other measurements (see supplemental materials [50], with integration times of around 10–16 hours per data point) for different input $g^{(2)}(0)$. While the model reproduces qualitatively the trend, there is a large point to point fluctuation that we attribute to low statistics and experimental fluctuations.

Our memory offers significant tunability in the write-in process that may prove useful in future hybrid quantum networks [55]. We start by showing that the memory can adapt to the input photon frequency. For that we vary the frequency of the control beam pulse. The maximum efficiency is observed for the two-photon resonance, see Fig. 5, achieving optimum storage conditions for the input photon. The width of the curve depends on the spectral properties of the input photon. Bandwidth-limited photons (i.e. photons that exhibit the minimum bandwidth for a given temporal duration) are desirable because one can achieve with them a high Hong-Ou-Mandel interference visibility [56] which is a requirement for most of the entanglement distribution protocols. Therefore, in order to benchmark the spectral properties of the input photon, we repeat the measurement with a weak coherent state (WCS) with the same waveshape, center frequency and mean number of photons. This WCS is derived from a laser exhibiting a linewidth much smaller than the bandwidth of the pulse. As can be seen in Fig. 5,

both spectra overlap very well suggesting that the input photon is close to bandwidth-limited.

We also study the bandwidth of our memory by sending WCS of different durations (with FWHM of 8 ns to 800 ns). We show the results in the supplemental materials [50] asserting that the memory can accommodate pulses of very different lengths without changing its efficiency.

Another interesting feature of the memory is that one can control how much of the input photon is absorbed and how much is transmitted. By varying the write-in control beam power one can change η_w as shown in Fig. 6 (top). This changes effectively the splitting ratio s/t between the stored and the transmitted photon pulse

$$\frac{s}{t} := \frac{\eta_{wr}}{1 - \eta_w} = \frac{p_s}{p_t}. \quad (2)$$

Our memory can therefore be used as a temporal beam splitter[57] with a tunable splitting ratio, which may have applications in the quantum repeater architecture mentioned in the introduction. To investigate this possibility, we plot s/t , see Fig. 6 (bottom). We see that s/t peaks for intermediate values of the write-in control beam powers and decays for higher values. This stands in contrast with the monotonically growing η_w and is a result of η_r decreasing with the control power. We attribute this behaviour of η_r to the asymmetrical distribution of the spin wave in the ensemble, when large write-in control powers are used [48, 58]. With increasing write power, the spin wave starts having more asymmetric shape, being mostly created at the beginning of the ensemble. This effect is known to limit the retrieval efficiency, especially in the forward retrieval configuration [48].

In Fig. 6 (bottom), we also plot the survival efficiency, defined as the probability of detecting a transmitted or stored photon per trial. We observe that it decreases with increasing control power due to the decrease of the

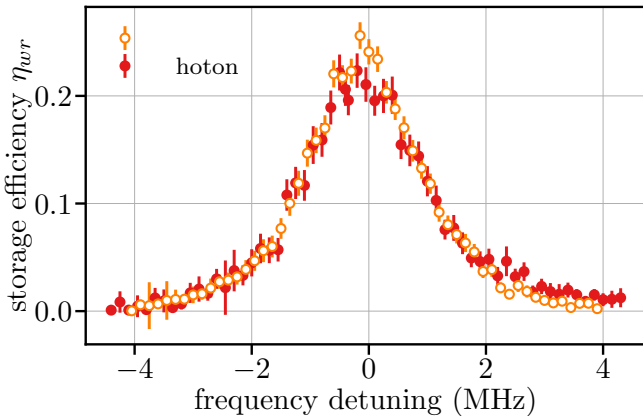


FIG. 5. Storage efficiency versus frequency detuning of the control write-in pulse for the single photon input (red) and WCS (orange). The frequency detuning is measured from the two-photon resonance of the input photon and the write-in control beam.

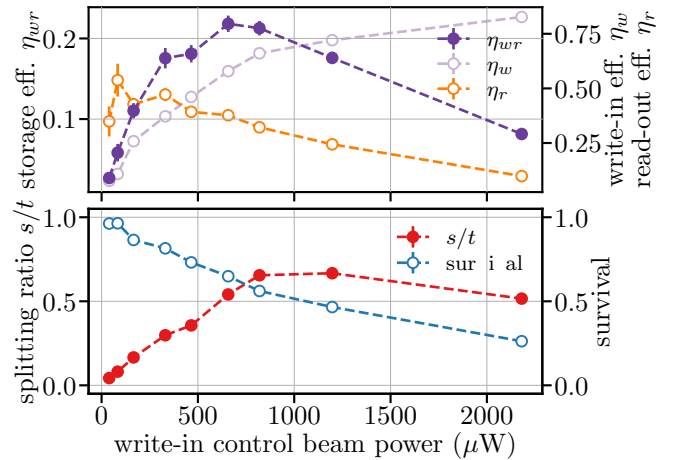


FIG. 6. Storage efficiency η_{wr} and related quantities as a function of the write-in control beam power. In the top panel we show the efficiencies η_w , η_r and η_{wr} and in the bottom panel we show the survival efficiency and s/t .

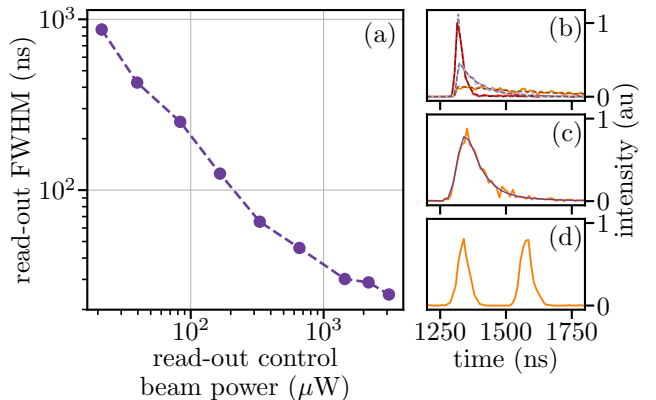


FIG. 7. Stored photon waveshape tunability. (a) Dependence of the stored photon duration on the read-out control beam power. (b) Selected waveshapes of the stored photons from (a) and their corresponding fits. (c) Stored photon waveshape (solid orange) matching exactly the input photon waveshape (dashed blue). (d) Stored photon shaped as a time-bin qubit.

read-out efficiency. With current conditions, the tunability range of s/t is limited, but we expect that backward retrieval should considerably improve the read-out efficiency at high write power, which will increase the survival probability [58]. As a first application of the single photon temporal beam splitter, we used the two temporal output modes of the memory to measure the antibunching parameter. For the measurement presented in Fig. 4, we obtain a $g^{(2)}(0) = 0.28(2)$ with a significantly increased count rate with respect to the case where we split each output mode with a standard BS.

Our memory also offers shape tunability of the stored photon [59]. In particular, one can retrieve photons with very different lengths (with FWHM of 25 ns to 900 ns) by changing the read-out control beam power, see Fig. 7(a,

b). We read out the memory with a square-shaped pulse resulting in a steep leading edge of the retrieved photon and slower decaying trailing edge. We fit the former with a Gaussian function and the latter with an exponential and obtain the total FWHM of the photon. One can also use more complex waveforms for the read-out control pulse to shape the read-out photon, e.g. reproducing the input photon or a time-bin qubit, see Fig. 7(c, d). This capability would allow for matching differently shaped photons emitted by different sources. We do not observe significant reduction of η_{wr} for different read-out pulse shapes, in agreement with theory [60].

IV. CONCLUSION

We demonstrated storage and retrieval of an on-demand single photon generated in one Rydberg-based atomic ensemble in another cold atomic ensemble through a Raman memory protocol. We achieved a 21 % memory efficiency and a signal-to-noise ratio up to 26 for the retrieved photon, leading to μ_1 of $1.00(7) \times 10^{-3}$. This allowed us to observe only a moderate degradation of the single photon statistics. We showed the adaptability of our memory in frequency and bandwidth. Moreover, we evaluated the performances of the built-in temporal beam splitter offered by the Raman memory. Lastly, we showed that we can shape the temporal waveform of the retrieved photon by shaping the read-out pulse power and waveform. These results are a step forward in the implementation of efficient quantum-repeater links using single-photon sources. In that context, one interesting advantage of having the source and the memory residing in different ensembles is that they can be optimized independently. This allows for an efficient single-photon generation and storage and facilitates the use of multiplexed quantum memories [16, 29], which would significantly improve repeater entanglement generation rates.

Several improvements should be applied to our experiment before it can become a practical alternative. The generation efficiency of the single photon from the Rydberg ensemble could be increased by increasing the OD

of the ensemble and/or by embedding the ensemble in a low finesse cavity [61]. The quality of the single photon (as measured by the autocorrelation function $g^{(2)}(0)$) could also be improved by addressing a slightly smaller ensemble and by reaching higher principal quantum number level to increase the Rydberg blockade radius, as was shown in [45], where $g^{(2)}(0)$ values smaller than 10^{-3} have been measured. Regarding the Raman quantum memory, higher storage and retrieval efficiencies could also be reached by increasing the OD of the ensemble [15] and using backward retrieval, or with an impedance matched cavity. Backward retrieval will also improve the survival probability and the performances of the temporal beam-splitter. Finally, longer storage time up to 1 s could be achieved by using magnetic insensitive transitions and by loading the ensemble into an optical lattice to suppress motional induced dephasing [62].

Note added. While finalizing our experiment, we learned about a recent experiment where a single photon generated by Rydberg atoms was stored in an atomic ensemble using electromagnetically induced transparency [63].

ACKNOWLEDGMENTS

We acknowledge interesting discussions with Gerhard Rempe.

L.H. and J.L. acknowledge funding from the European Unions Horizon 2020 research and innovation programme under the Marie Skłodowska-Curie grant agreement No. 713729.

This project received funding from the Government of Spain (PID2019-106850RB-I00 project funded by MCIN/AEI /10.13039/501100011033; Severo Ochoa CEX2019-000910-S), from the European Union's Horizon 2020 research and innovation program under Grant Agreement No. 899275 (DAALI), from the Gordon and Betty Moore Foundation through Grant No. GBMF7446 to H. d. R, from Fundació Cellex, Fundació Mir-Puig and from Generalitat de Catalunya (CERCA, AGAUR)

L.H. and J.L. contributed equally to this work.

[1] H. J. Kimble, The quantum internet, *Nature* **453**, 1023 (2008).

[2] H.-J. Briegel, W. Dür, J. I. Cirac, and P. Zoller, Quantum repeaters: The role of imperfect local operations in quantum communication, *Physical Review Letters* **81**, 5932 (1998).

[3] L.-M. Duan, M. D. Lukin, J. I. Cirac, and P. Zoller, Long-distance quantum communication with atomic ensembles and linear optics, *Nature* **414**, 413 (2001).

[4] N. Sangouard, C. Simon, H. de Riedmatten, and N. Gisin, Quantum repeaters based on atomic ensembles and linear optics, *Reviews of Modern Physics* **83**, 33 (2011).

[5] S. Ritter, C. Nölleke, C. Hahn, A. Reiserer, A. Neuzner, M. Uphoff, M. Mücke, E. Figueroa, J. Bochmann, and G. Rempe, An elementary quantum network of single atoms in optical cavities, *Nature* **484**, 195 (2012), 10.1038/nature11023.

[6] S. Langenfeld, P. Thomas, O. Morin, and G. Rempe, Quantum repeater node demonstrating unconditionally secure key distribution, *PRL* **126**, 230506 (2021).

[7] A. Stute, B. Casabone, P. Schindler, T. Monz, P. O. Schmidt, B. Brandstätter, T. E. Northup, and R. Blatt, Tunable ion-photon entanglement in an optical cavity, *Nature* **485**, 482 (2012), 10.1038/nature11120.

[8] D. Hucul, I. V. Inlek, G. Vittorini, C. Crocker, S. Debnath, S. M. Clark, and C. Monroe, Modular entangle-

ment of atomic qubits using photons and phonons, *Nature Physics* **11**, 37 (2015).

[9] V. Krutyanskiy, M. Meraner, J. Schupp, V. Krcmarsky, H. Hainzer, and B. P. Lanyon, Light-matter entanglement over 50?km of optical fibre, *npj Quantum Information* **5**, 72 (2019).

[10] L. J. Stephenson, D. P. Nadlinger, B. C. Nichol, S. An, P. Drmota, T. G. Ballance, K. Thirumalai, J. F. Goodwin, D. M. Lucas, and C. J. Ballance, High-rate, high-fidelity entanglement of qubits across an elementary quantum network, *PRL* **124**, 110501 (2020).

[11] T. Chanelière, D. N. Matsukevich, S. D. Jenkins, S.-Y. Lan, T. A. B. Kennedy, and A. Kuzmich, Storage and retrieval of single photons transmitted between remote quantum memories, *Nature* **438**, 833 (2005), 10.1038/nature04315.

[12] C. W. Chou, H. de Riedmatten, D. Felinto, S. V. Polyakov, S. J. van Enk, and H. J. Kimble, Measurement-induced entanglement for excitation stored in remote atomic ensembles, *Nature* **438**, 828 (2005).

[13] C.-W. Chou, J. Laurat, H. Deng, K. S. Choi, H. de Riedmatten, D. Felinto, and H. J. Kimble, Functional quantum nodes for entanglement distribution over scalable quantum networks., *Science (New York, N.Y.)* **316**, 1316 (2007).

[14] Z.-S. Yuan, Y.-A. Chen, B. Zhao, S. Chen, J. Schmiedmayer, and J.-W. Pan, Experimental demonstration of a BDCZ quantum repeater node, *Nature* **454**, 1098 (2008).

[15] M. Cao, F. Hoffet, S. Qiu, A. S. Sheremet, and J. Laurat, Efficient reversible entanglement transfer between light and quantum memories, *Optica* **7**, 1440 (2020).

[16] L. Heller, P. Farrera, G. Heinze, and H. de Riedmatten, Cold-Atom Temporally Multiplexed Quantum Memory with Cavity-Enhanced Noise Suppression, *Physical Review Letters* **124**, 210504 (2020).

[17] Y. Yu, F. Ma, X.-Y. Luo, B. Jing, P.-F. Sun, R.-Z. Fang, C.-W. Yang, H. Liu, M.-Y. Zheng, X.-P. Xie, W.-J. Zhang, L.-X. You, Z. Wang, T.-Y. Chen, Q. Zhang, X.-H. Bao, and J.-W. Pan, Entanglement of two quantum memories via fibres over dozens of kilometres, *Nature* **578**, 240 (2020).

[18] P. C. Humphreys, N. Kalb, J. P. J. Morits, R. N. Schouten, R. F. L. Vermeulen, D. J. Twitchen, M. Markham, and R. Hanson, Deterministic delivery of remote entanglement on a quantum network, *Nature* **558**, 268 (2018).

[19] M. K. Bhaskar, R. Riedinger, B. Machielse, D. S. Levonian, C. T. Nguyen, E. N. Knall, H. Park, D. Englund, M. Lončar, D. D. Sukachev, and M. D. Lukin, Experimental demonstration of memory-enhanced quantum communication, *Nature* **580**, 60 (2020).

[20] H. de Riedmatten, M. Afzelius, M. U. Staudt, C. Simon, and N. Gisin, A solid-state light-matter interface at the single-photon level, *Nature* **456**, 773 (2008), 10.1038/nature07607.

[21] M. P. Hedges, J. J. Longdell, Y. Li, and M. J. Sellars, Efficient quantum memory for light, *Nature* **465**, 1052 (2010).

[22] E. Saglamyurek, N. Sinclair, J. Jin, J. A. Slater, D. Oblak, F. Bussieres, M. George, R. Ricken, W. Sohler, and W. Tittel, Broadband waveguide quantum memory for entangled photons, *Nature* **469**, 512 (2011), 10.1038/nature09719.

[23] C. Clausen, I. Usmani, F. Bussieres, N. Sangouard, M. Afzelius, H. de Riedmatten, and N. Gisin, Quantum storage of photonic entanglement in a crystal, *Nature* **469**, 508 (2011), 10.1038/nature09662.

[24] D. Lago-Rivera, S. Grandi, J. V. Rakonjac, A. Seri, and H. de Riedmatten, Telecom-heralded entanglement between multimode solid-state quantum memories, *Nature* **594**, 37 (2021).

[25] X. Liu, J. Hu, Z.-F. Li, X. Li, P.-Y. Li, P.-J. Liang, Z.-Q. Zhou, C.-F. Li, and G.-C. Guo, Heralded entanglement distribution between two absorptive quantum memories, *Nature* **594**, 41 (2021).

[26] C. Simon, H. de Riedmatten, M. Afzelius, N. Sangouard, H. Zbinden, and N. Gisin, Quantum repeaters with photon pair sources and multimode memories, *Physical Review Letters* **98**, 190503 (2007).

[27] O. A. Collins, S. D. Jenkins, A. Kuzmich, and T. A. B. Kennedy, Multiplexed memory-insensitive quantum repeaters, *Physical Review Letters* **98**, 060502 (2007).

[28] S.-Y. Lan, A. G. Radnaev, O. A. Collins, D. N. Matsukevich, T. A. Kennedy, and A. Kuzmich, A multiplexed quantum memory, *Optics Express* **17**, 13639 (2009).

[29] Y. Pu, N. Jiang, W. Chang, H. Yang, C. Li, and L. Duan, Experimental realization of a multiplexed quantum memory with 225 individually accessible memory cells, *Nature Communications* **8**, 15359 (2017).

[30] W. Chang, C. Li, Y.-K. Wu, N. Jiang, S. Zhang, Y.-F. Pu, X.-Y. Chang, and L.-M. Duan, Long-distance entanglement between a multiplexed quantum memory and a telecom photon, *Physical Review X* **9**, 041033 (2019).

[31] D. Felinto, C. W. Chou, J. Laurat, E. W. Schomburg, H. de Riedmatten, and H. J. Kimble, Conditional control of the quantum states of remote atomic memories for quantum networking, *Nature Physics* **2**, 844 (2006).

[32] N. Sangouard, C. Simon, M. Afzelius, and N. Gisin, Analysis of a quantum memory for photons based on controlled reversible inhomogeneous broadening, *Physical Review A: Atomic, Molecular, and Optical Physics* **75**, 032327 (2007).

[33] A. Seri, A. Lenhard, D. Rieländer, M. Gündoğan, P. M. Ledingham, M. Mazzera, and H. de Riedmatten, Quantum correlations between single telecom photons and a multimode on-demand solid-state quantum memory, *Physical Review X* **7**, 021028 (2017), arXiv:1701.09004.

[34] Y. Wang, J. Li, S. Zhang, K. Su, Y. Zhou, K. Liao, S. Du, H. Yan, and S.-L. Zhu, Efficient quantum memory for single-photon polarization qubits, *Nature Photonics* **13**, 346 (2019).

[35] N. Akopian, L. Wang, A. Rastelli, O. G. Schmidt, and V. Zwiller, Hybrid semiconductor-atomic interface: Slowing down single photons from a quantum dot, *Nature Photonics* **5**, 230 (2011).

[36] P. Siyushev, G. Stein, J. Wrachtrup, and I. Gerhardt, Molecular photons interfaced with alkali atoms, *Nature* **509**, 66 (2014).

[37] J.-S. Tang, Z.-Q. Zhou, Y.-T. Wang, Y.-L. Li, X. Liu, Y.-L. Hua, Y. Zou, S. Wang, D.-Y. He, G. Chen, Y.-N. Sun, Y. Yu, M.-F. Li, G.-W. Zha, H.-Q. Ni, Z.-C. Niu, C.-F. Li, and G.-C. Guo, Storage of multiple single-photon pulses emitted from a quantum dot in a solid-state quantum memory, *Nature communications* **6**, (2015).

[38] T. Kroh, J. Wolters, A. Ahlrichs, A. W. Schell, A. Thoma, S. Reitzenstein, J. S. Wildmann, E. Zallo, R. Trotta, A. Rastelli, O. G. Schmidt, and O. Benson, Slow and fast single photons from a quantum dot inter-

acting with the excited state hyperfine structure of the Cesium D1-line, *Scientific Reports* **9**, 13728 (2019).

[39] M. Lettner, M. Mücke, S. Riedl, C. Vo, C. Hahn, S. Baur, J. Bochmann, S. Ritter, S. Dürr, and G. Rempe, Remote entanglement between a single atom and a bose-einstein condensate, *PRL* **106**, 210503 (2011).

[40] Y. O. Dudin and A. Kuzmich, Strongly interacting rydberg excitations of a cold atomic gas, *Science (New York, N.Y.)* **336**, 887 (2012).

[41] D. Maxwell, D. J. Szwier, D. Paredes-Barato, H. Busche, J. D. Pritchard, A. Gauguet, K. J. Weatherill, M. P. A. Jones, and C. S. Adams, Storage and control of optical photons using Rydberg polaritons, *Physical Review Letters* **110**, 1 (2013).

[42] L. Li and A. Kuzmich, Quantum memory with strong and controllable Rydberg-level interactions, *Nature Communications* **7**, 13618 (2016).

[43] J. Li, M.-T. Zhou, C.-W. Yang, P.-F. Sun, J.-L. Liu, X.-H. Bao, and J.-W. Pan, Semideterministic entanglement between a single photon and an atomic ensemble, *PRL* **123**, 140504 (2019).

[44] L. Li, Y. O. Dudin, and A. Kuzmich, Entanglement between light and an optical atomic excitation., *Nature* **498**, 466 (2013).

[45] D. P. Ornelas-Huerta, A. N. Craddock, E. A. Goldschmidt, A. J. Hachtel, Y. Wang, P. Bienias, A. V. Gorshkov, S. L. Rolston, and J. V. Porto, On-demand indistinguishable single photons from an efficient and pure source based on a Rydberg ensemble, *Optica* **7**, 813 (2020).

[46] A. Padrón-Brito, J. Lowinski, P. Farrera, K. Theophilo, and H. de Riedmatten, Probing the indistinguishability of single photons generated by Rydberg atomic ensembles, *Physical Review Research* **3**, 033287 (2021).

[47] M. D. Lukin, M. Fleischhauer, R. Cote, L. M. Duan, D. Jaksch, J. I. Cirac, and P. Zoller, Dipole blockade and quantum information processing in mesoscopic atomic ensembles, *Physical Review Letters* **87**, 037901 (2001).

[48] J. Nunn, I. A. Walmsley, M. G. Raymer, K. Surmacz, F. C. Waldermann, Z. Wang, and D. Jaksch, Mapping broadband single-photon wave packets into an atomic memory, *Physical Review A: Atomic, Molecular, and Optical Physics* **75**, 011401 (2007).

[49] B. Albrecht, P. Farrera, G. Heinze, M. Cristiani, and H. de Riedmatten, Controlled rephasing of single collective spin excitations in a cold atomic quantum memory, *Physical Review Letters* **115**, 160501 (2015).

[50] *See Supplemental Material at (URL Will Be Inserted by Publisher) for (Give Brief Description of Material).*

[51] J. Wolters, G. Buser, A. Horsley, L. Béguin, A. Jöckel, J.-P. Jahn, R. J. Warburton, and P. Treutlein, Simple atomic quantum memory suitable for semiconductor quantum dot single photons, *Physical Review Letters* **119**, 060502 (2017).

[52] S. E. Thomas, T. M. Hird, J. H. D. Munns, B. Brecht, D. J. Saunders, J. Nunn, I. A. Walmsley, and P. M. Ledingham, Raman quantum memory with built-in suppression of four-wave-mixing noise, *Physical Review A: Atomic, Molecular, and Optical Physics* **100**, 033801 (2019).

[53] M. Namazi, C. Kupchak, B. Jordaan, R. Shahrokhsahi, and E. Figueira, Ultralow-noise room-temperature quantum memory for polarization qubits, *Physical Review Applied* **8**, 034023 (2017).

[54] M. Gündoğan, P. M. Ledingham, K. Kutluer, M. Mazzera, and H. de Riedmatten, Solid state spin-wave quantum memory for time-bin qubits, *Physical Review Letters* **114**, 230501 (2015).

[55] N. Maring, P. Farrera, K. Kutluer, M. Mazzera, G. Heinze, and H. De Riedmatten, Photonic quantum state transfer between a cold atomic gas and a crystal, *Nature* **551**, 485 (2017).

[56] C. K. Hong, Z. Y. Ou, and L. Mandel, Measurement of subpicosecond time intervals between two photons by interference, *Physical Review Letters* **59**, 2044 (1987).

[57] K. F. Reim, J. Nunn, X.-M. Jin, P. S. Michelberger, T. F. M. Champion, D. G. England, K. C. Lee, W. S. Kolthammer, N. K. Langford, and I. A. Walmsley, Multipulse Addressing of a Raman Quantum Memory: Configurable Beam Splitting and Efficient Readout, *Physical Review Letters* **108**, 263602 (2012).

[58] A. V. Gorshkov, A. Andre, M. D. Lukin, and A. S. Sørensen, Photon storage in Lambda-type optically dense atomic media. II. Free-space model, *Physical Review A: Atomic, Molecular, and Optical Physics* **76**, 033805 (2007).

[59] P. Farrera, G. Heinze, B. Albrecht, M. Ho, M. Chávez, C. Teo, N. Sangouard, and H. de Riedmatten, Generation of single photons with highly tunable wave shape from a cold atomic ensemble, *Nature Communications* **7**, 13556 (2016).

[60] J. Nunn, *Quantum Memory in Atomic Ensembles*, Ph.D. thesis, University of Oxford (2008).

[61] C.-W. Yang, J. Li, M.-T. Zhou, X. Jiang, X.-H. Bao, and J.-W. Pan, Single-shot measurement of a Rydberg superatom via collective photon burst, arXiv:2106.10858 [quant-ph] (2021), comment: 6 pages, 4 figures, arXiv:2106.10858 [quant-ph].

[62] X.-J. Wang, S.-J. Yang, P.-F. Sun, B. Jing, J. Li, M.-T. Zhou, X.-H. Bao, and J.-W. Pan, Cavity-enhanced atom-photon entanglement with subsecond lifetime, *PRL* **126**, 090501 (2021).

[63] Y. Yu, P.-F. Sun, Y.-Z. Zhang, B. Bai, Y.-Q. Fang, X.-Y. Luo, Z.-Y. An, J. Li, J. Zhang, F. Xu, X.-H. Bao, and J.-W. Pan, Measurement-device-independent verification of a quantum memory, *PRL* **127**, 160502 (2021).

Supplementary Material:

Ultra-low noise quantum memory for quasi-deterministic single photons generated by Rydberg collective atomic excitations

L. Heller,¹ J. Lowinski,¹ K. Theophilo,¹ A. Padrón-Brito,¹ and H. de Riedmatten^{1,2}

¹*ICFO - Institut de Ciències Fotoniques, The Barcelona Institute of Science and Technology, Castelldefels (Barcelona) 08860, Spain*

²*ICREA-Institució Catalana de Recerca i Estudis Avançats, 08015 Barcelona, Spain*

I. ESTIMATION OF μ_1 PARAMETER (WITH SINGLE PHOTON INPUT)

An important figure of merit for a quantum memory is the parameter μ_1 , which is defined as the minimum mean number of input photons to have a signal-to-noise ratio (SNR) of 1 for the stored photon.

In Fig. 1 we show a measurement of SNR in the read-out (stored) detection window by varying the mean number of single photons at the input of the Raman memory. This is achieved by varying the Rydberg probe power (see Fig. 2 of the main text). From a linear fit that passes through zero, we estimate a μ_1 parameter of $1.00(7) \times 10^{-3}$.

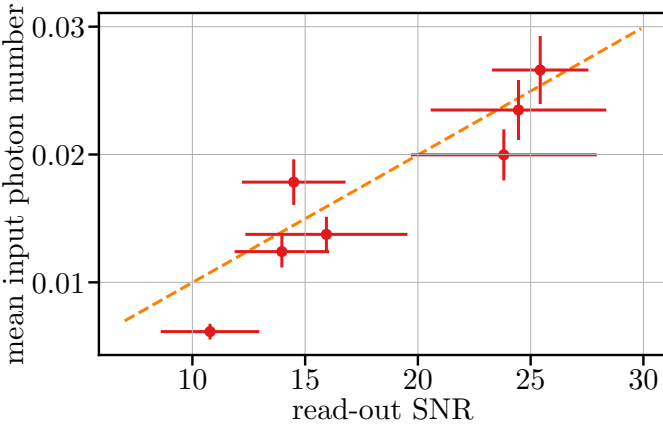


FIG. 1. Mean number of single photons at the input of the memory as a function of the read-out SNR. Orange dashed line: linear fit that passes through zero. The slope of this line corresponds to μ_1 .

II. ACCEPTANCE MEMORY BANDWIDTH (WITH WEAK COHERENT STATES)

To understand whether the memory efficiency is limited by its acceptance bandwidth, we measure the storage and retrieval efficiency for input pulses with variable duration. The maximum duration of the single photons generated at the source is limited by the dephasing rate of the collective Rydberg excitations. Moreover, the minimum duration is limited by the coupling beam power,

leading to FWHM greater than ~ 90 ns. Therefore, we instead send weak coherent state (WCS) pulses with mean number of photons well below 1. The duration of the WCS pulses is controlled by an acousto-optic modulator (AOM), achieving pulses as short as 8 ns (FWHM). We send Gaussian-shaped pulses, because the conversion to bandwidth is straightforward.

The results are shown in Fig. 2. For pulse durations between 25 ns and 750 ns, the total efficiency η_{wr} remains constant and is in agreement with the efficiencies measured for the single-photon input. Only for pulse durations below 25 ns, corresponding to a bandwidth of about ≈ 17.6 MHz (assuming transform-limited Gaussian pulses), the storage and retrieval efficiency drops. We attribute this drop to limited control power and finite AOM rise time, resulting in a smaller pulse area. For input pulses much longer than 750 ns (not characterised here), the efficiency is expected to be eventually limited by the lifetime of the memory [1]. We estimate the bandwidth of the single photon to be approximately 4 MHz, assuming bandwidth-limited Gaussian pulses.

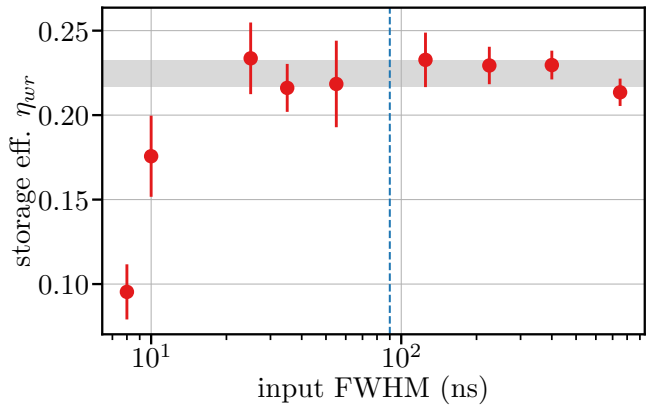


FIG. 2. Storage and retrieval efficiency η_{wr} as a function of the temporal duration (FWHM) of WCS input pulses with Gaussian shape. Grey horizontal shaded area represents the mean (0.225) and standard deviation (0.008) of the efficiency for input pulse durations above 25 ns. Blue dashed vertical line represents the minimum duration of the single photon generated by the Rydberg-based source (~ 90 ns FWHM). For each data point, write-in control pulse power, shape and delay are optimized.

III. MEMORY PERFORMANCE WITH OPTICAL DEPTH (WITH WEAK COHERENT STATES)

It is instructive to analyse the memory performance when varying optical depth (OD), since OD governs how efficiently the incoming light pulse is absorbed and re-emitted. For that, we vary the trapping laser power during the magneto-optical trap stage and used the shortest interrogation time possible to be able to scan the full range of OD available.

The OD value is obtained by measuring the transmission of a continuous coherent beam around resonance with the $|g_s\rangle \rightarrow |e_s\rangle$ transition. Results are shown in Fig. 3. The storage efficiencies are measured for WCS pulses as input, shaped to mimic the temporal profile of the single photons generated in the Rydberg-based source.

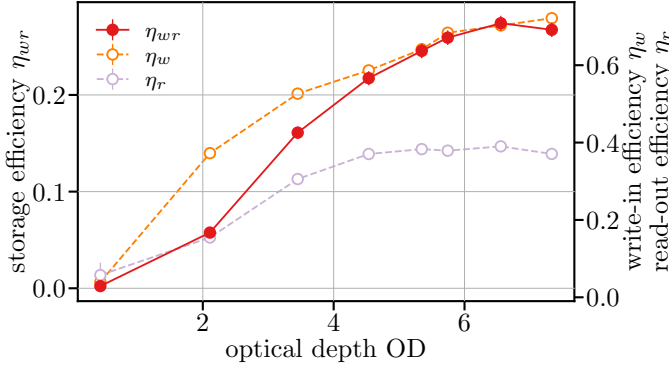


FIG. 3. Storage efficiencies η_w , η_r and η_{wr} as a function of the optical depth of the ensemble for weak coherent input pulses with a mean photon number of 0.077. For each data point, the write-in control pulse power and the delay are optimized.

We observe a saturation of the storage and retrieval efficiency $\eta_{wr} = \eta_w \cdot \eta_r$ for OD around 6.5. However, the write-in efficiency η_w seems to still profit from higher OD, while read-out efficiency η_r is already at the maximum. One possible explanation for this behaviour is re-emission followed by re-absorption, which limits the maximal retrieval efficiency in forward retrieval (i.e. when the photon field is retrieved from the medium co-propagating to the input) [2, 3].

Data in the main text was taken for OD around 5, which constitutes a compromise between achieving high η_{wr} while at the same time maintaining an acceptable duty cycle for data acquisition.

IV. EFFECT OF THE NOISE IN THE MEASURED AUTOCORRELATION FUNCTION OF SINGLE PHOTONS

Noise originated either from the control beam or its interaction with the ensemble can lead to uncorrelated co-

incidences that affect the measured single-photon statistics of the transmitted or stored photon. In the absence of control field and atoms, the unperturbed autocorrelation is measured as:

$$g_{\text{in}}^{(2)}(0) = \frac{c_{1,2}}{p_1 p_2}, \quad (1)$$

where p_1 (p_2) is the probability of detection per trial on detector 1(2), and $c_{1,2}$ is the probability of coincidence detection per trial between both detectors. When a storage attempt is performed, the noise introduced by the control pulses and the atoms alter the probabilities for detection and coincidences as follow:

$$\tilde{c}_{1,2} = c_{1,2} + p_1 p_{n,2} + p_2 p_{n,1} + p_{n,1} p_{n,2} \quad (2)$$

$$\tilde{p}_{1(2)} = p_{1(2)} + p_{n,1(2)}. \quad (3)$$

Here, $p_{n,1}$ ($p_{n,2}$) is the noise probability for detector 1(2). The autocorrelation is therefore:

$$\begin{aligned} g_{\text{out}}^{(2)}(0) &= \frac{\tilde{c}_{1,2}}{\tilde{p}_1 \tilde{p}_2} \\ &= \frac{p_{12} + p_1 p_{n,2} + p_2 p_{n,1} + p_{n,1} p_{n,2}}{p_1 p_2 + p_{n,1} p_2 + p_{n,2} p_1 + p_{n,1} p_{n,2}}, \end{aligned} \quad (4)$$

which can be rewritten in terms of SNRs as

$$g_{\text{out}}^{(2)}(0) = \frac{g_{\text{in}}^{(2)}(0) + 1/\text{SNR}_1 + 1/\text{SNR}_2 + 1/(\text{SNR}_1 \text{SNR}_2)}{1 + 1/\text{SNR}_1 + 1/\text{SNR}_2 + 1/(\text{SNR}_1 \text{SNR}_2)}, \quad (5)$$

where $\text{SNR}_{1(2)} = p_{1(2)}/p_{n,1(2)}$ is the signal-to-noise ratio for detector 1(2).

Assuming that SNR is the same for both detectors, this expression finally simplifies to

$$g_{\text{out}}^{(2)}(0) = \frac{g_{\text{in}}^{(2)}(0) + 2/\text{SNR} + 1/\text{SNR}^2}{1 + 2/\text{SNR} + 1/\text{SNR}^2}. \quad (6)$$

In Fig. 4, we characterize the effect of noise on the $g^{(2)}(0)$ of the stored and the transmitted photons for different values of $g^{(2)}(0)$ of the input photon (i.e. with no storage attempt). The input $g^{(2)}(0)$ was scanned by varying the mean number of photons in the probe (see Fig. 2 in the main text). We can see that, in general, the output $g^{(2)}(0)$ degrades compared to the input $g^{(2)}(0)$ and that the autocorrelation of the transmitted photon is better than the one of the stored photon. Therefore, we can conclude that the model qualitatively reproduces the expected trend. We attribute the imperfection in the quantitative analysis to low statistics and experimental fluctuations.

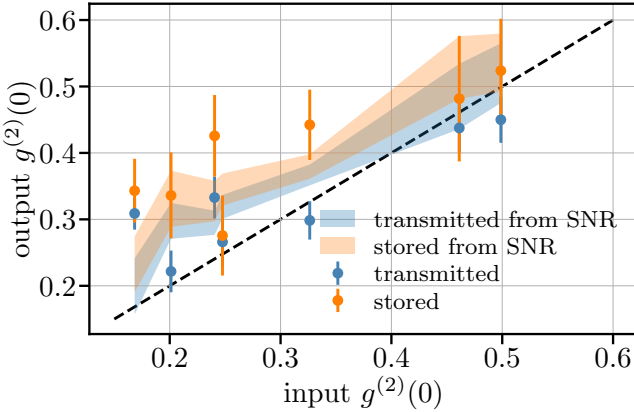


FIG. 4. Output $g^{(2)}(0)$ of the transmitted and the stored photons as a function of the input $g^{(2)}(0)$. Dashed black line: autocorrelation after the memory equals input. Shaded areas: autocorrelation for transmitted and stored photon as expected from eq. 6, taking into account uncertainty in $g_{\text{in}}^{(2)}(0)$ and SNR.

[1] P. Farrera, G. Heinze, B. Albrecht, M. Ho, M. Chávez, C. Teo, N. Sangouard, and H. de Riedmatten, Generation of single photons with highly tunable wave shape from a cold atomic ensemble, *Nature Communications* **7**, 13556 (2016).

[2] K. F. Reim, J. Nunn, V. O. Lorenz, B. J. Sussman, K. C. Lee, N. K. Langford, D. Jaksch, and I. A. Walmsley, Towards high-speed optical quantum memories, *Nat Photon* **4**, 218 (2010), 10.1038/nphoton.2010.30.

[3] A. V. Gorshkov, A. Andre, M. Fleischhauer, A. S. Sørensen, and M. D. Lukin, Universal approach to optimal photon storage in atomic media, *Physical Review Letters* **98**, 123601 (2007).